Stefan Hiermaier
Editor

Predictive Modeling of Dynamic Processes

A Tribute to Professor Klaus Thoma

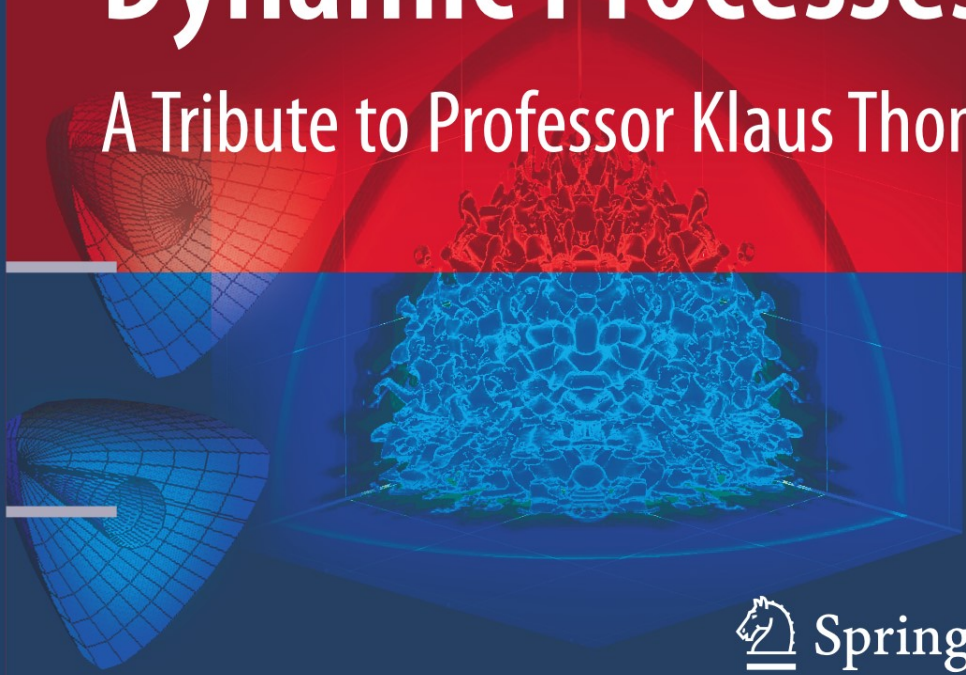

Springer

Chapter 16
Numerical Analysis Method for the RC Structures Subjected to Aircraft Impact and HE Detonation

Masahide Katayama and Masaharu Itoh

Abstract This paper proposes and demonstrates a numerical simulation method suitable to analyze the local damage and dynamic response of the structures composed of the reinforced concrete (RC) and/or the geological materials subjected to the severe impulsive loading by the aircraft impact and the high explosive detonation. After the brief description about the numerical simulation method, the former part of this work attests that the present method has an enough accuracy to simulate the dynamic behavior of the RC structures subjected to the impulsive loading, through the comparison of the numerical analysis results with those of reference experiments. In the latter part of this work, three-dimensional numerical simulation results are investigated which were performed by using the basically the same analysis method as applied in the former part, but for much more complicated physical system. Through the discussion on the numerical simulation results the effectiveness of the present method is demonstrated from the viewpoint of the high-velocity impact safety, the explosion safety, and the structural integrity evaluation.

16.1 Introduction

Recently the serious hazards have increased such that terrorists attack various public buildings and structures by using high explosives (HE). At the same time, another type of hazards cannot be ignored, i.e. the hazards caused by the industrial accidents in use of the energetic materials like reactive gas mixtures as well as high explosives. Since these hazards are not small-size problems, it is indispensable to discuss as

Masahide Katayama
Impact Dynamics Team, ITOCHU Techno-Solutions, 2-5, Kasumigaseki 3-chome, Chiyoda-ku, Tokyo 100-6080, Japan e-mail: masahide.katayama@ctc-g.co.jp

Masaharu Itoh
Impact Dynamics Team, ITOCHU Techno-Solutions, 2-5, Kasumigaseki 3-chome, Chiyoda-ku, Tokyo 100-6080, Japan e-mail: masaharu.itoh@ctc-g.co.jp

S. Hiermaier (ed.), *Predictive Modeling of Dynamic Processes,*
DOI 10.1007/978-1-4419-0727-1_16,

interactions between the energetic materials and the constructional structures. However, these problems consist of highly non-linear and complex physical systems so that numerical analyses for such problems, especially in the three-dimensional model, can never have been solved until around a decade ago except for a few huge computer systems in the world. Both hardware and software are now available in order to solve some of such difficult problems, not to say sufficient.

From another viewpoint, an accident previously considered hypothetical became real when the hijacked Boeing 767 passenger jet crashed into the North Tower of the New York World Trade Center on 11th September, 2001. The possibilities of aircraft impacts against infrastructures have been investigated mainly in nuclear industries since 80's [1, 2, 3]. However, the aircrafts discussed in these studies were not commercial jetliners but military jet fighters such as an F-4 Phantom.

In the meantime, the concrete and geological materials indicate complicated behaviors in the compressive and the tensile region, especially when subjected to the severe impact or impulsive loading. Therefore, a number of material properties are necessary to describe such highly nonlinear and dynamic phenomena. On the other hand, it is general that only the limited properties are measured in the usual material test of theses materials, i.e. limited to density, elastic moduli and static compressive strength. So it is of great use, if the present scheme provides us the recommended values of the dynamic material properties based on the correlation between the static compressive strength and the other properties. The author and others have proposed and improved such constitutive and failure models for over ten years [4, 5], and K. Thoma et al. also have been developed their own model for the concrete referred to as the RHT model [6] .

In this paper we proposes and demonstrates a numerical simulation method by using these two material models suitable to analyze the local damage and dynamic response of the structures composed of the reinforced concrete (RC) and/or the geological materials subjected to impulsive loading by the aircraft impacts and the HE detonations.

16.2 Analytical Method

16.2.1 Analysis Code

A multiple solver type hydrocode: AUTODYN [7, 8] is used for the numerical simulation conventional, Godunov-type and FCT (Flux-Corrected Transport)], the ALE (Arbitrary Lagrangian-Eulerian), the SPH (Smoothed Particle Hydrodynamics), the shell and the beam solvers, moreover the interactions among these solvers can be taken into account in a problem. These solvers are compared and investigated in

order to clarify what solver is the most suitable and efficient to model the individual part of the present problem: the concrete, the reinforcement, the soil/sand, the air and the HE, etc. The three-dimensional calculation for such complex physical system is very heavy even for the current advanced computers. The modeling method for the actual problems is proposed from the practical viewpoint that we persist in using not so expensive but easily obtainable and easily usable computers.

16.2.2 Material Models

The material model in AUTODYN consists of two parts: i) the equation of state (E.O.S.) describes the relationship among pressure (p), density (ρ) and internal energy (e) as indicated by Eq. (16.1), and ii) the material strength model does the constitutive relation including the failure model, as many hydrocodes do.

$$p = F(\rho, e)\ . \tag{16.1}$$

In the low-velocity structural analyses, the Young's modulus (E) and the Poisson ratio (ν) are used for the solid materials. And the bulk modulus (K) is derived by Eq. (16.2), so that the usage of E and ν is just equivalent to that of K.

$$K = \frac{E}{3(1-2\nu)} \tag{16.2}$$

Considering that the definition of the bulk modulus is given by Eq. (16.3), this can be recognized as using the simplest EOS, i.e. the proportional (linear) E.O.S. to the density and neglecting the energy term,

$$p = -K\frac{dV}{V_{ref}} = K\left(\frac{\rho}{\rho_{ref}} - 1\right) \tag{16.3}$$

where V is the volume and subscript 'ref' denotes reference variable.

In this study, we applied the linear E.O.S. sometimes to the concrete in the interests of simplicity, and did all the times to the beam and shell elements, because the change of density cannot be taken into account in these elements. The porous E.O.S. was applied sometimes to the concrete and all the times to the soil, but we leave out its detailed descriptions because limitations of space here.

The numerical erosion model is not exactly a physical material model, but it is very useful to model the cratering and spalling (scabbing) of the solid materials, as well as the scattering of the liquid materials in the Lagrangian frame of reference. During the subsequent calculations, some of the Lagrangian elements can become grossly distorted and, unless some remedial action is taken, can seriously impair the

progress of the calculation. Therefore, procedures have been incorporated into AUTODYN to remove such Lagrangian elements from the calculation, if a pre-defined strain exceeds a specified limit. When an element is removed from the calculation process in this way the mass within the element can either be discarded or distributed to the corner nodes of the element. If the mass is retained, conservation of inertia and spatial continuity of inertia are maintained. However the compressive strength and internal energy of the material within the element are lost whether or not the mass is retained.

In AUTOYDN, Lagrangian grids can impact and slide along any Lagrangian surface, at the same time, this surface can be dynamically redefined as the surface changes through the numerical erosion. Erosion is a technique wherein Lagrangian elements are transformed into free mass points not connected to the original element. These free nodes can optionally further interact with other bodies or the original body from which they were eroded. This feature allows the study of impact interaction problems including deep penetrations in the low to hypervelocity range using a Lagrangian technique.

16.2.2.1 Concrete

We adopted two-parameter Drucker-Prager criterion instead of the four- or five-parameter failure surface used by Han and Chu in the static non-uniform hardening plasticity model [9]. In this paper we show the numerical results only on a relatively high-velocity ($> 100m/s$) impact problem as a concrete structure. However, we demonstrated and verified in other opportunity that the present material model (referred to as DYCAP model) is also applicable to the lower velocity impact problems of the concrete [5].

To describe dynamic behavior of fragile material such as concrete is complicated because it shows highly nonlinear behaviour and its multi-axial behaviour is hard to be measured by the experiment. Many constitutive equations of concrete were proposed until now, but the only few ones can predict dynamic behaviour of concrete in the multi-axial stress state, and the applicable region are often very limited. We are concerned with two constitutive equations that can be applicable to the multi-axial stress state. One is Drucker-Prager's equation that shows good results in the region of high strain rate. Another is Han & Chen's non-uniform hardening plasticity model that can be applied to the region of low strain rate. We combined both equations together to establish a new constitutive model (DYCAP), introducing strain rate dependency and strain hardening to this. In this model yield surface is described by:

$$f = \sigma_y - s\left(k_{0c}, k_{0t}, p\right)\ \sigma_y^d = 0 \tag{16.4}$$

where σ_y is yield stress, σ_y^d is the ultimate stress surface that is Drucker-Prager's criterion, s is the shape factor that describes non-uniform hardening behaviour, p is hydrostatic pressure, k_{0c} is the hardening parameter for compression, and k_{0t} is the hardening parameter for tension.

To incorporate the strain rate effect, the dynamic compressive strength $\hat{f}_c'$ and the dynamic tensile strength $\hat{f}_t'$ proposed by Yamaguchi et al.[10] are introduced to the Drucker-Prager's equation as shown in Eq. (16.5) and (16.6).

$$\hat{f}_c'(\dot{\varepsilon}) = \left[1.021 - 0.05076\log\dot{\varepsilon} + 0.2583\left(\log\dot{\varepsilon}\right)^2\right] f_c' \tag{16.5}$$

$$\hat{f}_t'(\dot{\varepsilon}) = \left[0.8267 - 0.02987\log\dot{\varepsilon} + 0.04379\left(\log\dot{\varepsilon}\right)^2\right] f_t' \tag{16.6}$$

where $\dot{\varepsilon}$ is strain rate $\dot{\varepsilon} = \sqrt{\left(2/3\right)\dot{\varepsilon}_{ij}\dot{\varepsilon}_{ij}}$ and strain rate tensor $\dot{\varepsilon}_{ij}$.

The strain hardening effect is incorporated by use of the shape factor s, which is a function of hardening factors: k_{0c} and k_{0t}. The shape factor $s$is defined in the three different regions in the same manner as Chen's method [11], that is in the tensile region, I the transitional region, and in the compression region. The detailed equation is found in the literature by Itoh et al. [4]. The typical relation between yield stress and pressure in the DYCAP model is shown in Fig. 16.1 . The curve is arranged by $\varepsilon_t/\varepsilon_t^{'d}$ where ε_t is the largest tensile strain in its history and $\varepsilon_t^{'d}$ is the dynamic ultimate tensile strain.

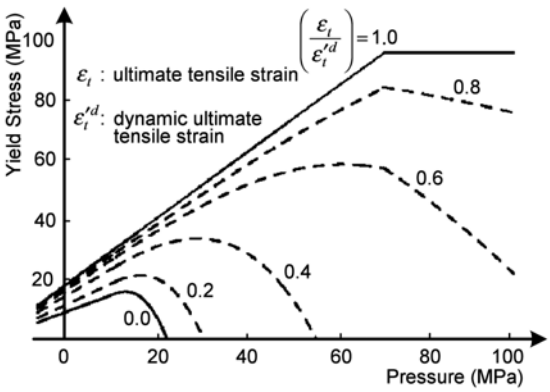

Fig. 16.1 Typical relation between yield stress and pressure in the DYCAP model.

16.2.2.2 High explosives (HE)

We applied the JWL equation of state to the HE proposed by Lee et al. [12], and using programmed 'on-time burning' model assuming the ideal stationary detonation. The equation of state is shown in Eq. (16.7), and the detonation properties and the parameters of the JWL equation for many high explosives have been compiled by Dobratz et al. for a couple of decades [13].

$$p = A_{JWL}\left(1-\frac{\omega\eta}{R_1}\right)\exp\left(-\frac{R_1}{\eta}\right) \quad + B_{JWL}\left(1-\frac{\omega\eta}{R_2}\right)\exp\left(-\frac{R_2}{\eta}\right) + \omega\eta\rho_{ref}e \tag{16.7}$$

where $\eta = \rho/\rho_{ref}$ and A_{JWL}, B_{JWL}, R_1, R_2, ω are the material properties of the HE. In the handbook [13], the other important variables like the detonation velocity (V_det) and the initial internal energy (e_0) are also included. The constitutive model of the HE is neglected, namely assumed to be hydrodynamic.

16.2.2.3 Ductile materials

It has been known that a linear relationship between the shock velocity (U_s) and the particle velocity (u_p), as shown by Eq. (16.8), can adequately represent the Hugniot relation for many condensed materials which impact at velocities less than the threshold for shock-induced vaporization.

$$U_s = c_0 + s_1 u_p \tag{16.8}$$

where c_0 and s_1 are experimentally determined material constants and c_0 denotes the bulk sound velocity. Then the following Mie-Grüneisen form of the shock Hugoniot E.O.S. is derived by assuming Grüneisen Γ as shown in the Eq. (16.10) of [14]:

$$p = p_{ref}(\rho) + \rho\Gamma\left\{e(\rho) - e_{ref}(\rho)\right\} \tag{16.9}$$

$$\Gamma \equiv \frac{1}{\rho}\left(\frac{\partial p}{\partial e}\right)_{\rho} \tag{16.10}$$

This equation of state is not only recognized to be applicable for a wide variety of solid and liquid materials, but also the material data of the E.O.S. for many materials are published by not a few research organizations [15].

In the Johnson-Cook constitutive model applied mainly to ductile materials, the yield stress (Y) is estimated by the function of strain (ε), strain rate ($\dot{\varepsilon}$) and homologous temperature (T^*) defined by Eq. (16.12).

$$Y = (A_{J-C} + B_{J-C}\varepsilon^n)(1 + C_{J-C} ln\dot{\varepsilon}^*)(1 - T^{*m}) \tag{16.11}$$

where $\dot{\varepsilon}^* = \dot{\varepsilon}/\dot{\varepsilon}_0$ is the dimensionless plastic strain rate for $\dot{\varepsilon}_0 = 1.0 s^{-1}$,

$$T^* \equiv \frac{T - T_{room}}{T_{melt} - T_{room}} \tag{16.12}$$

and T_{room} and T_{melt} are the room temperature and melting temperature, respectively. The variables: A_{J-C}, B_{J-C}, C_{J-C}, m and n are determined by an experimental procedure [12]. However, the thermal term is neglected for the beam and shell solvers, because no volume changes, consequently no temperature changes, of the elements are calculated in these solvers.

16.3 Numerical Analyses

16.3.1 Missile Impact on RC Structure (2D)

16.3.1.1 Numerical analysis models

In order to verify the present material model of the concrete, we carried out a number of numerical analyses [4] to simulate an experimental test program conducted by Muto et al. [2]. The main purpose of the reference test is to investigate the local damage of the reinforced concrete structure caused by the accidental aircraft impact on the nuclear related protective structures. The test program consists of three scale models for F-4 Phantom fighter: 1/7.5-, 1/2.5- and full-scale models. Two types of projectiles, i.e. rigid and deformable, were adopted to model the engine part of the aircraft in the experiment.

Although the target RC structures are square in the experiment, two-dimensional axisymmetric model was used in the numerical analysis so that the targets may be assumed to be the circular plates with the equivalent sectional areas. The parts of concrete material were modeled by the Lagrangian frame of the reference, shell elements were applied to the reinforcement and the thin parts of the 1/7.5-scale deformable missile as shown in Fig. 16.2. Therefore, the reinforcement was also modeled by the thin circular plate with the equivalent mass. It should be noted that the bending moment was taken into account for the shell elements in the missile, while was ignored for the shell element modeling the reinforcement, i.e. was assumed to be membrane. Each lower half indicates the numerical mesh used in the calculation in Fig. 16.2. The concrete plate was constrained at the radial end to both the axial and radial directions. To the interface between the missile and the RC structure, the slide/impact interactive boundary condition without friction was applied, and all the elements in the concrete, missile and reinforcement were also enabled

to interact with the elements that exist in the same component after subjected to a serious deformation. The capabilities of the interaction and the numerical erosion triggered by the maximum geometric strain enable us to simulate the complicated deformation processes. For Lagrangian elements the erosion strains 100 to 500 % were used, while the erosion strains equivalent to the ultimate physical (material) strains were applied for shell and beam elements, because there do not occur any bulk deformations in the case of these two- or one-dimensional elements.

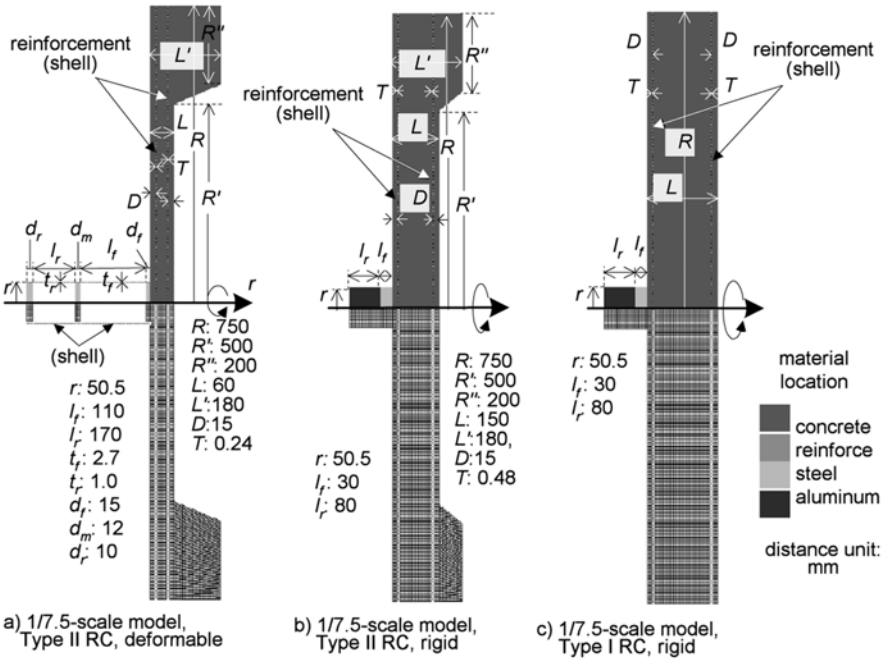

Fig. 16.2 Geometrical models and numerical meshes in the analysis.

16.3.1.2 Numerical results

Only the results of the 1/7.5-scale model are discussed in this paper, and the cases and results in both the experiment and the numerical analysis are summarized in Fig. 16.3, 16.4 and Table 16.1 for the selected 1/7.5 model tests reported in the references [2]. Both results are compared in their residual velocities of the projectiles, in the vertical/horizontal/average diameters of the front craters and rear scabbing of the target plates, and in the overall damage status of the target plates. The numerical results can be considered to simulate the overall deformations of the reinforced con-

crete panels, because the present numerical results nearly predict both the cratering in the front side and the scabbing (spalling) in the rear side.

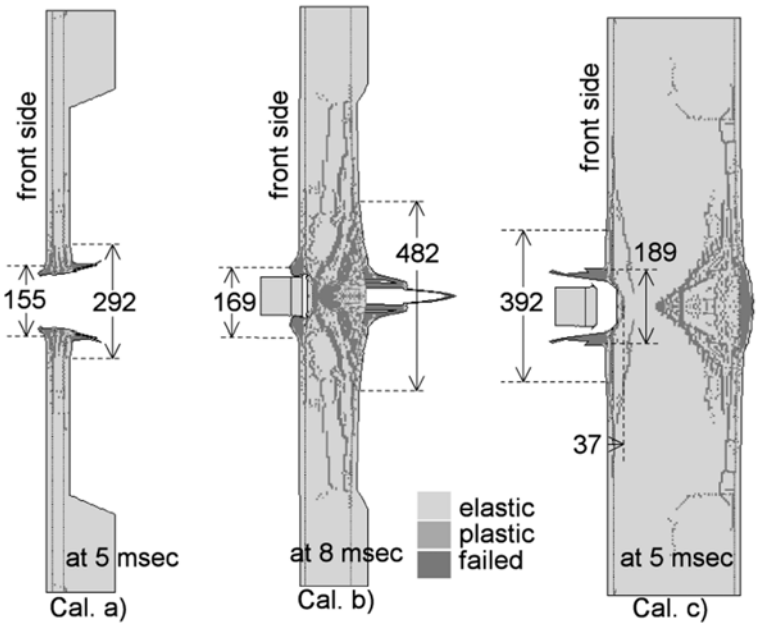

Fig. 16.3 Numerical results for the 1/7.5-scale model cases.

Table 16.1 Conditions and results of the 1/7.5 model comparing between the calculations (C) and the experiments(E).

ID	C/E	T^* (mm)	V_{imp}^{**} (m/s)	V_{res}^{***} (m/s)	Projectile	Front Diameter ver. (mm)	hor. (mm)	av. (mm)	Depth (mm)	Rear Diameter ver. (mm)	hor. (mm)	av. (mm)	Status
a)	C	60	194	138	deformable	–	–	155	–	–	–	292	perforated
1-1	E	60	194	143	deformable	178	171	175	–	420	335	378	perforated
b)	C	150	143	-1.94	rigid	–	–	169	32.3	–	–	482	scabbing
1-3	E	150	143	N/A	rigid	155	185	170	N/A	590	440	515	scabbing
c)	C	350	198	-11.8	rigid	–	–	189	37	–	–	–	perforated
1-8	E	350	198	N/A	rigid	320	302	311	42	–	–	–	perforated

*: Thickness **: Impact Velocity ***: Residual Velocity
ver.: vertical hor.:horizontal av.:average

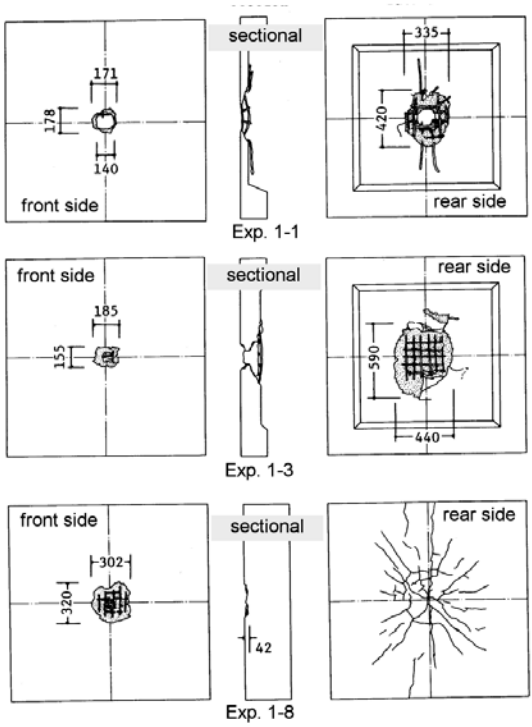

Fig. 16.4 Experimental results for the 1/7.5-scale model cases.

16.3.2 HE Detonations On and Near the RC Slab (2D & 3D)

16.3.2.1 Analysis models

The effects of the detonation on RC slabs have been investigated experimentally, when the HE is placed and detonated on the surface of the RC slab [17, 18, 19, 20]. Some numerical studies on the damage of the RC slabs subjected to the contact HE detonation have also conducted over the comparison with the experimental results [17, 21, 22]. However, almost all numerical analyses are carried out by two-dimensional models until recently. The reason of such a limitation seems to have come from both the computational hardware and software capabilities as they were, when those studies were conducted.

In the experiment by Kraus et al. [17], the RC slab has the dimensions 2.0 2.0 0.3 m with a concrete compressive strength of 44 to 48 MPa, and has a percentage of reinforcement of 42 kg/m2. The cubic high explosive is placed in the center of and directly on the slab. The used HE is PETN with a mass of 1.0 kg and the

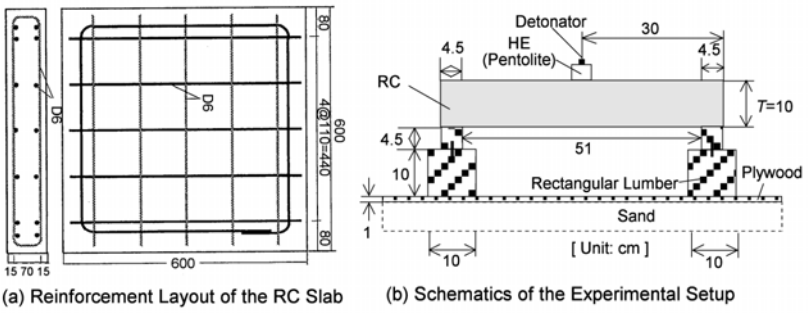

Fig. 16.5 Configuration of the HE detonation test on the RC slab by Tanaka et al.

density of 1.5 g/cm3. In the calculation, the concrete, reinforcement and HE were modeled by the Lagrangian element. Next, Fig. 16.5 depicts the configuration of one of a series of HE detonation tests on the RC slab conducted by Tanaka et al. [19]. We performed a three-dimensional calculation to simulate this experimental condition. In this calculation, the concrete and HE were modeled by the Lagrangian element with the numerical erosion capability, while the reinforcement was done by the beam element, by using finer numerical discretization than the previous calculation. The numerical grids used in the present calculation are indicated in Fig. 16.6.

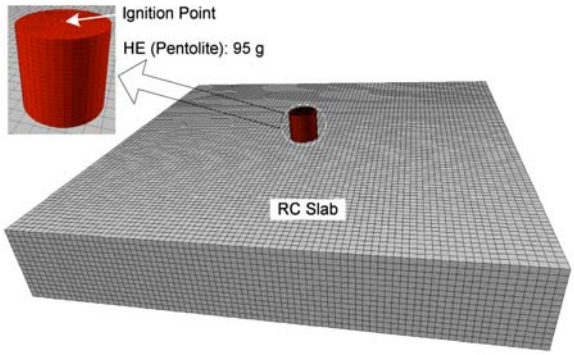

Fig. 16.6 Three-dimensional numerical grids to simulate the HE detonation test on RC slab by Tanaka et al.

The compressive strength of the concrete measured 28-day later is 56 MPa, and the reinforcement has the yield strength of 300 MPa and the tensile strength of 419 MPa. The cylindrical HE with a diameter of 41.8 mm is placed in the center of and directly on the slab. The HE is the pentolite with a mass of 95 g.

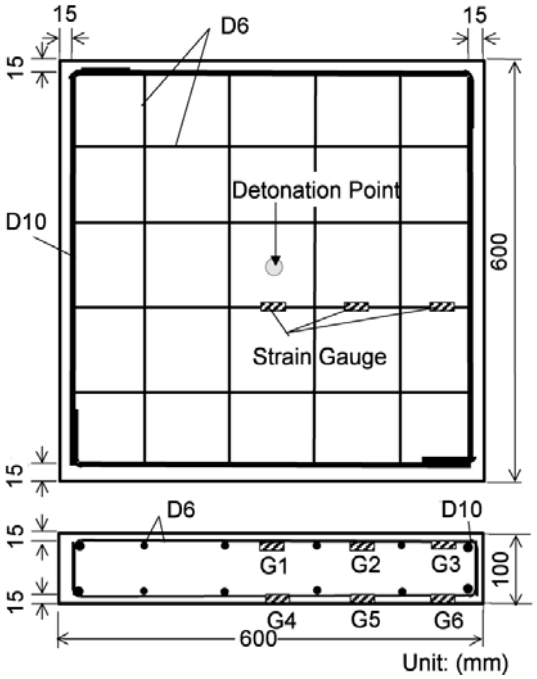

Fig. 16.7 Reinforcement Layout of the the RC slab by Morishita et al.

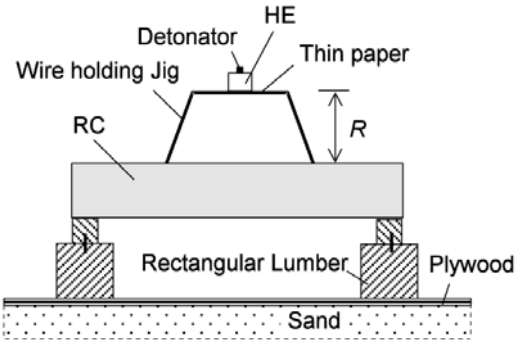

Fig. 16.8 Setup of the Experiments by Morishita et al.

Thirdly, Morishita et al. conducted another type of HE detonation tests near the RC slab, in which the HE are placed in the center of RC slabs but at the position standoff from the surface of RC slab [20]. Figures 16.7 and 16.8 indicate the configuration for the tests. It should be noted that the alignment of the reinforcements is different from the above mentioned contact explosion experiment, especially that there are no reinforcements at the center of the RC slab. We also performed two numerical simulations for this type of experiment: with the standoffs of 100 mm and 50 mm. In these calculations, the concrete was modeled by the Lagrangian element with the numerical erosion capability, the reinforcement was done by the beam element, as they were modeled in the contact explosion calculation. However, the HE was modeled by the Eulerian frame of reference, and the atmosphere was taken into account by the same numerical grid that the HE was modeled.

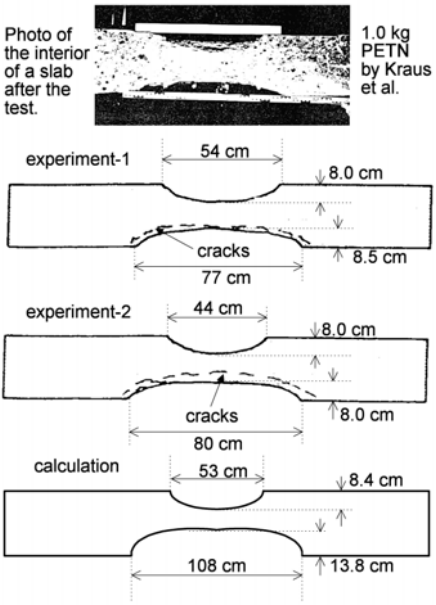

Fig. 16.9 Comparison of the present 3-D calculation with the experimental results by Kraus et al.

The main parts of these numerical simulations were carried out in the three-dimensional model, after a preliminary axisymmetric two-dimensional calculation to simulate the pentolite detonation and its propagation process in the atmosphere with the initial pressure of 101.3 kPa. The preliminary calculation was carried out by using the multiple-material Eulerian solver. Then, the two-dimensional distribution of the physical properties of the pentolite products and air at the final stage was

remapped to the three-dimensional analysis model as an initial condition. All the pentolite products are assumed to be in the gas phase at this moment.

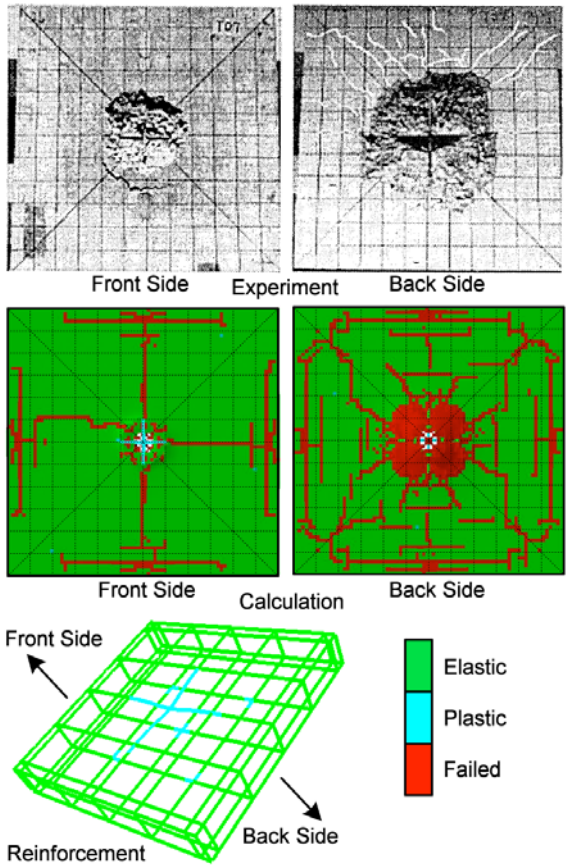

Fig. 16.10 Comparison of the 3-D calculation of the HE detonation on RC slab with the experimental results by Tanaka et al.

In the three-dimensional calculation we applied FCT-Euler solver to the gas materials (pentolite products and air), because this solver is suitable to model the shock in the gas and is much faster than the multiple-material Eulerian solver. The Euler-Lagrange interactive boundary condition was applied to the front surfaces of the RC slab. In order to attain this motivation, the E.O.S. for the pentolite was switched from the JWL equation to the ideal gas equation (as shown in Eq. (13) as well as the air, and the pentolite products were assumed to have the same ratio of specific

heat (γ) of 1.4 just same as the air, because the third term of the JWL E.O.S. is equivalent to the ideal gas E.O.S., after perfectly burned.

$$p = (\gamma - 1)\,\rho\, e \tag{16.13}$$

16.3.2.2 Numerical results

First, Fig. 16.9 shows the schematic comparison of the three-dimensional calculation, which was performed in 1997 by the authors, with the experimental results conducted by Kraus et al. This three-dimensional calculation was carried out by using relatively coarse numerical discretization in today's environment, so that the deformed slab obtained by the calculation does not have so smoothed outline. The schematic deformation in Fig. 16.9 only represents the typical parameters: i.e. the diameters and depths of front and rear craters.

Secondly, Fig. 16.10 shows the comparison of the damage of the RC slab between the calculation and the experiment in the front and back sides for the Tanaka's experiment. The calculational result seems to evaluate the crater diameters in both sides a little bit smaller than the experiment, but the overall damage of the RC slab in the calculation indicates a fairly good agreement with the experiment. Especially, the calculation successfully simulates the exposure of the reinforcement in the front side and the pattern of the crack extension in the back side.

The lower figure depicts the damage and deformation of the reinforcement in a three-dimensional bird's-eye view by removing the concrete grid. Thirdly, Fig. 16.11 depicts the remapping procedure from two-dimensional model to three-dimensional one for the Morishita's experiment: the upper contours show the pressure distributions and the lower ones do the density distributions. There appear no material boundaries in the three-dimensional contours, because we assumed that pentolite products in gas phase and air are the same material.

The comparison between the experimental and calculational results of the standoff explosion is shown in Fig. 16.12. Only very shallow craters are observed on the front side in both experimental and calculational results of the 100-mm-standoff case, whereas obvious craters appear in the 50-mm-standoff case. Calculational results successfully simulate the spalling and cracking behaviours on the back side as well as the damages in the central cross section, in comparison with the corresponding photos in the experiment for the 50-mm-standoff case, especially these results might be characterized by the crack patterns both along the reinforcements and in the radial directions. All the beam elements modeling reinforcements seem to remain in the elastic state, differently from the result of contact explosion.

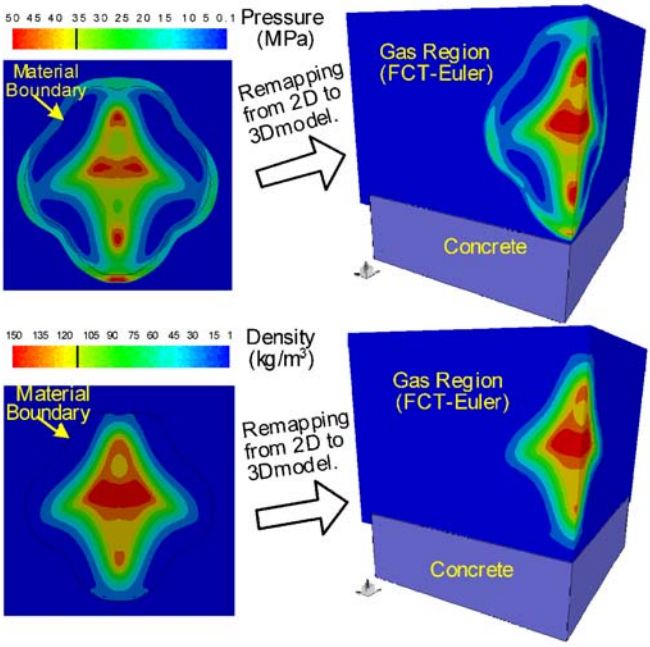

Fig. 16.11 Remapping procedure from 2D/multiple-material Euler to 3D/FCT-Euler model.

16.3.3 F-4 Phantom Crashing on a RC Wall (3D)

16.3.3.1 Analysis Model

Next reference experiment was performed by Sandia National Laboratories on the terms of the contract with the Muto Institute of Structural Mechanics, Inc. in Japan [2, 3]. This experiment is situated as a full-scale model one of a series of impact tests mentioned in the section 16.3.1. The experiment yielded an extensive set of response data, of which we focus on the following main measurements,

1) Crushing behaviour of the F-4 Phantom,
2) Impact force loaded on the RC target structure,
3) Damage on the concrete.

Recommendations for future studies are also presented to improve the accuracy of the proposed model. Before describing the numerical simulation we briefly summarize the impact test. The primary purpose of the test was aimed at determining the impact force as a function of time when an F-4 Phantom impacts onto a massive, essentially rigid, reinforced concrete. Figure 16.13 is the instantaneous photograph of the impact.

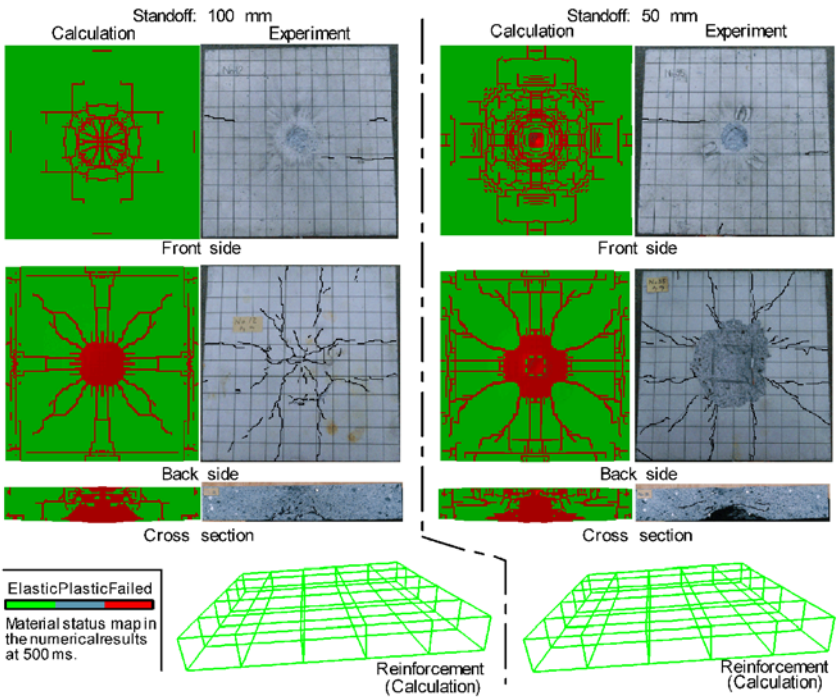

Fig. 16.12 Comparison of the 3-D calculation of the HE detonation on RC slab with the experimental results by Morishita et al.

Fig. 16.13 The instantaneous photograph of the F-4 impacting the target (Courtesy of Sandia National Laboratories).

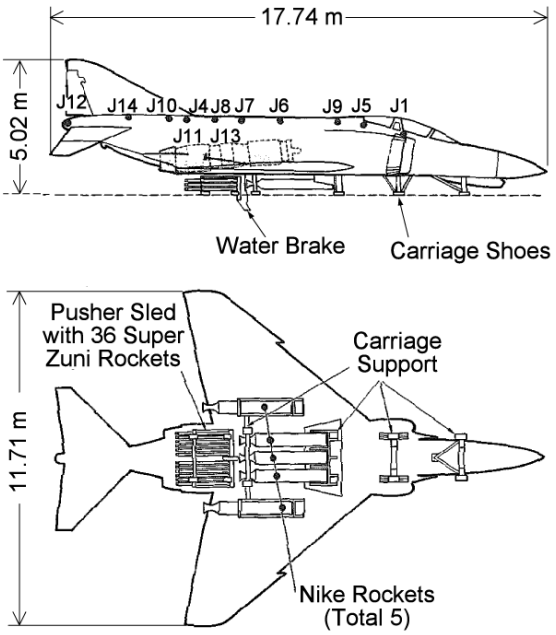

Fig. 16.14 Test configuration of F-4 Phantom [16].

The test configuration of the F-4 is shown in Fig. 16.14. The front and the main landing gears were removed. Instead a sled with a carriage structure was attached on the under surface of the aircraft. The sled was mounted on two rails of 600 meter long which guided the F-4, accelerated by rockets, to the target. The impact speed was adjusted to 215 m/s. Note that the shape and layout of the fuel tanks were not available, when this project started in 2004.

The total impact weight was 19 tones comprising 12.7 tones of the F-4, 1.5 tones of the sled and the carriage, 4.8 tones of water which is used to simulate the weight of fuel. The weight specification is listed in Table 16.2. The target was a rectangular block of reinforced concrete 7 meter square and 3.66 meter thick which weighs 469 tones (i.e. approximately 25 times heavier than the F-4). It was placed on an air-bearing platform which enabled almost free movement in the direction of impact. The geometry of the fuselage of the F-4 Phantom is created first by the general-purpose mesh generation computer program TrueGrid [23]. Then the obtained geometry is imported into the finite element model of the AUTODYN as shown in the left-hand side of Fig. 16.15. The size of the F-4 is adjusted to fit to the configurations shown in Fig. 16.14.

Table 16.2 Specification of the impact weight.

Components	Test (t)	Simulation (t)
Fuselage and Wings, etc.	9.2	9.3
Engines	3.5	3.4
Water	4.8	4.8
Rocket and Sled	1.5	–
(Total)	19.0	17.5

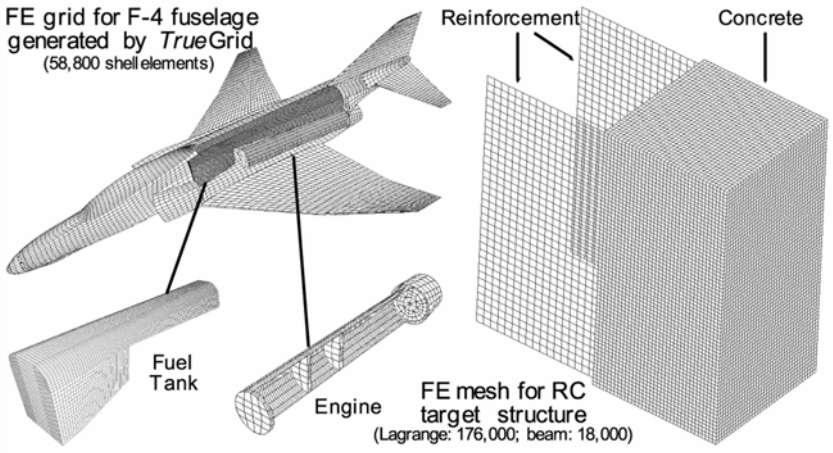

Fig. 16.15 Geometrical models of the F-4 Phantom and the RC target structure.

Because of the severe impact loading condition a constitutive model for the material of the aircraft is required to consider the strain hardening and the strain rate effects. The Johnson-Cook model [24] was adopted and the material properties of the 2024-T351 aluminium were taken from the material library of AUTODYN. The material properties of Glass-Epoxy for the windshield were also taken from the same library. Most components of the aircraft were modeled by shell elements except the engines and the water inside the fuel tanks. They were discretized by solid elements. We adopted the simple model for the engine which was designed for and used by the separate impact test [2] as shown in the lower middle of Fig. 16.15 because the actual GE-J79 engine is too complicated to consider. The material properties of the engine were also taken from the same reference.

As mentioned above the shape and layout of the fuel tanks were not provided in the test report, we refer to [25] in order to place it inside the fuselage in the improved model carried out in 2005. The lower left-hand side of Fig. 16.15 shows the mesh of the tank in which water is filled with. The surface nodes of the water were rigidly joined with the corresponding ones of the tank. The following material properties were used for the water: density of kg/m3, bulk modulus of 2.25 GPa and spall strength of -2.5 MPa.

We adopted a numerical method to scale the density of the aluminium which is increased by four times that of the actual one. Without this technique the thickness of the fuselage and the wings should be specified as 16 mm in order to match the weight of 9.2 tones. We assume that a reasonable thickness is about one forth of it. Hence the density is scaled up in order to save the computer time to improve the Courant condition.

The concrete wall is divided uniformly as shown in the right-hand side of Fig. 16.15. Each element is approximately a cube of 0.1 meter. In order to represent the material nonlinearity of the concrete we adopt the RHT [6] model which has the following specific features like pressure hardening, strain hardening, strain rate hardening and damage with tensile crack softening. The properties are taken from the material library of the AUTODYN and calibrated with the compressive strength of 23.5 MPa.

Also shown in Fig. 16.15 are the reinforcing bars which are modeled by beam elements. The ratio of reinforcement of the test is 0.4 %. The same ratio is applied to the model. The following material properties of the steel [16] are used: Young's modulus of 206 GPa, Poisson's ratio of 0.3, yield strength of 490 MPa, ultimate strength of 740 MPa and ultimate strain of 0.19.

In the test, it was observed that each wing tip and a portion of tail were sheared off due to the impact, and the other parts were completely destroyed. Pieces of the aircraft and lumps of crushed engines were found in the wide area. A sequence of images recorded by high speed cameras at the test site displayed that the main wings were severed by the edges of the target.

16.3.3.2 Numerical results

Figure 16.16 shows the deformed mesh configurations after impact. The aircraft collapses from the front section as if it impacts into a rigid wall. Most of the finite elements are numerically eroded because of large deformations. Only remained are the pieces of the fuselage, the portions of the tail wings, the thickened parts of the

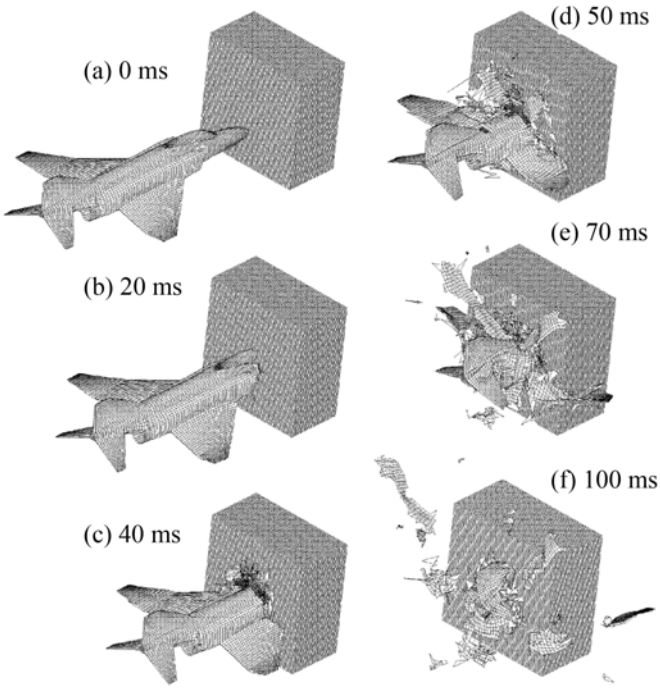

Fig. 16.16 Sequence of the impact and deformation of F-4 and RC structure.

engines (Fig. 16.17(c)) and the tip of main wings. These results reproduce successfully the crushing behaviour of the aircraft observed in the test.

The impact force histories obtained by the test and by two sorts of simulation are compared in Fig. 16.18. The case not modeling the fuel tanks (old one) underestimates the impact force, as well as its peak shifts to the right-hand side. On the other hand, the case modeling the fuel tanks (new one) simulates the impact force history by the experiment fairly well in the shape, magnitude and timing. This agreement is brought about by the feature of the numerical model, namely, the mass distributions of the engines and water are approximately reproduced, and the sum of the weight of these components amounts to almost half the weight of the aircraft, neglecting the differences caused by not modeling the rockets, sled, etc. Note that the head of fuel tanks is located before that of the engine, and that this fact causes the appearance of the peak of the impact force in the new model. The impact force of the calculation is evaluated by differentiating the momentum response of the whole RC structure by time. The obtained transient curve is then shifted 8 ms to the origin (left) in order to compare its peaks with the test ones.

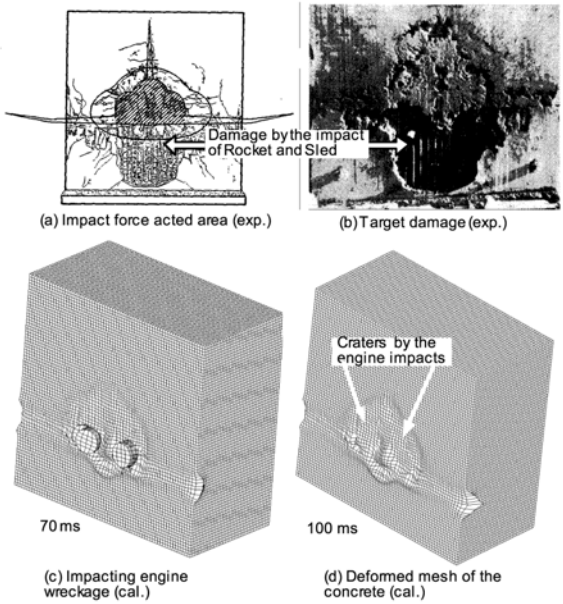

Fig. 16.17 The Damage aspect on the RC structure by the calculation (cal.) and the experiment (exp.).

The impact of the engines caused craters like two 'eyes' [2]. The formation of the craters are illustrated by (c) and (d) of Fig. 16.17. The crater depth (60 mm) reported in the experiment is slightly shallower than that obtained in the calculation (65 mm). The impact of the fuselage inflicted only minor damage on the target to form a shallow dent on the surface in both the experiment and the calculation. The distinct shape like a flattened 'pear' is formed similarly in both results. The impact of the rockets and sled caused major damage to the concrete in the lower part. But this cannot be reproduced by the calculation justifiably, as they were not taken into account in the present calculation.

16.3.4 Boeing 747 Jet Impacting on Thick Concrete Walls (3D)

16.3.4.1 Analysis models

The objective of this work is to numerically asses the damage of the wall caused by the impact of the B747 which is almost 15 times heavier than the F-4. All the components of the jetliner in our numerical model, namely, the fuselage, the wings and the engines were modeled by shell elements. The five different types of targets were assumed to be reinforced or non-reinforced concrete walls with three differ-

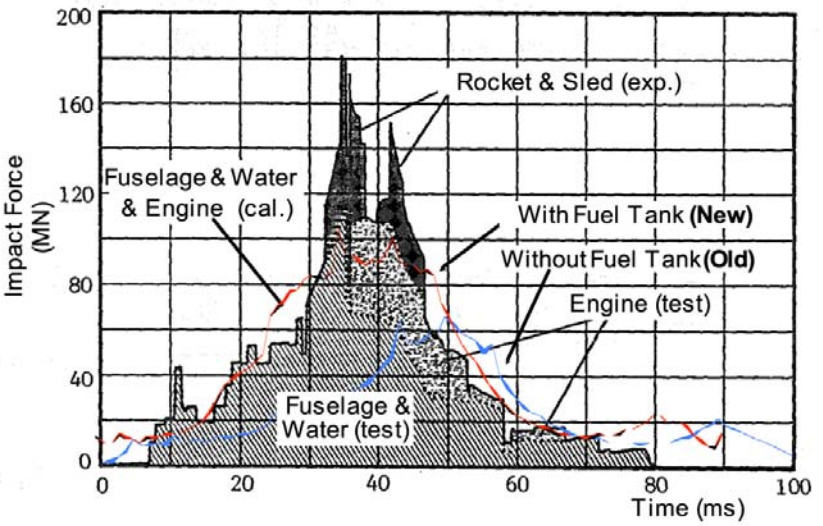

Fig. 16.18 The impact force histories loaded to the RC structure by the calculation (cal.) and the experiment (exp.).

ent thicknesses, additionally a rigid wall case was also carried out. The impacts between these elements were taken into account by using a contact capability. An eroding slide-line capability was utilized to prevent mesh tangling.

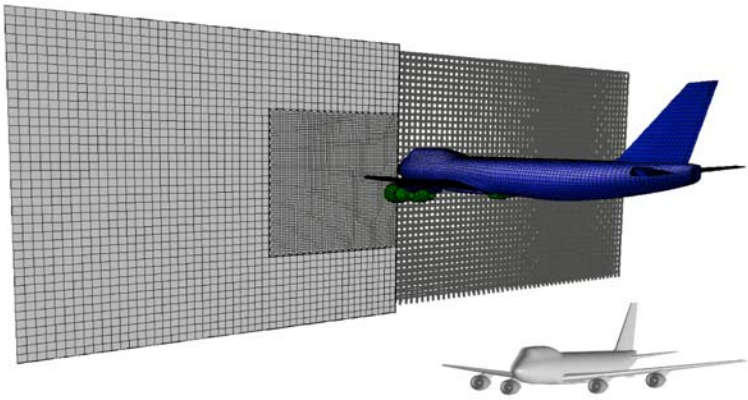

Fig. 16.19 Geometrical grid and model of B747 and RC wall in the calculation.

The shell solver was applied to the jetliner, the hexahedral solid solver to the concrete wall, and the beam solver to the reinforcement by using AUTODYN-3D. The geometry of the jetliner is created as a first step by using TrueGrid in a similar way of the F-4 Phantom model. Then the obtained geometry was imported into the AUTODYN finite element model as shown in Fig. 16.19. The overall length is 70.5 m and the wing span is 64.0 m. The thickness of the shell elements was adjusted so that the numerical model was consistent with the actual Boeing 747 [[26]. The total mass of the jetliner is thus 3.4105 kg (340 t) including four engines and the fuel. The impact velocity of the jetliner was assumed to be 83.3 m/s (300 km/h) which slightly exceeds the landing speed of about 77.8 m/s (280 km/h). Because of the intense impact loading condition, a constitutive model for the material of the jetliner is required to take into consideration both the strain hardening and strain rate effects. The Johnson-Cook model is adopted and the material properties of the 2024-T351 aluminum are taken from a reference [16].

Table 16.3 Numerical analysis cases.

Case Name	Wall Thickness	Reinforcement
CASE-1	1 m	0.8%
CASE-2	2 m	0.8%
CASE-3	2 m	None
CASE-4	3 m	0.8%
CASE-5	3 m	None
CASE-6	Rigid	–

Six cases of numerical analyses were carried out for different types of targets as shown in Table 16.3. All the concrete targets have rectangular shapes with the same 150 m width and 60 m height. As indicated in the left-hand side of Fig. 16.19 for the CASE–4, fine meshes were assigned to the central region where the impact loading is concentrated while coarse meshes were used for the surrounding region. The fine region has a face of 60 m30 m and a thickness of 3 m which consists of 1206015 meshes. The size of one solid element is then 0.5 m0.5 m0.2 m. The surrounding region was divided uniformly into rectangular solid elements. Each element has a size of 1.5 m1.5 m0.2 m. The concrete wall has 186,000 solid elements totally.

In order to represent the material nonlinearity of the concrete we adopted the RHT [6] model which has the following specific features like pressure hardening, strain hardening, strain rate hardening and damage with tensile crack softening. The material properties calibrated with the compressive strength of 35 MPa were taken from the material library of AUTODYN. The bottom of the wall was rigidly fixed, while no boundary condition was applied to the other five surfaces.

The right-hand side of Fig. 16.19 also depicts the double-reinforced arrangement. The number of longitudinal rebars is 99 and that of lateral ones is 39. They are placed 0.4 meter inside the front surface of the wall. The same number of bars is put along the back surface. The ration of the reinforcement is corresponding to 0.8 percent. The following material properties were used for the reinforcement: density of 7.8103 kg/m3: bulk modulus of 1.71105 MPa: shear modulus of 7.88105 MPa: yield stress of 2.15102 MPa: fracture strain of 0.19.

16.3.4.2 Numerical results

Figure 16.20 summarizes the overview on the numerical results of the present study for five different target walls except for CASE–6, while each assumption for the impactor (jetliner) is the same. The calculations of CASE–1 through CASE–5 were carried out up to 1 s and CASE–6 was done up to 0.6 s. The figures of (a-1) through (c-1) depict the deformations or damages estimated to the jetliners and the concrete walls in the impact side and the back side, for the CASE–1 through CASE–3 respectively, as well as the figures of (d–1) through (f–1) do in the impact side and from the upper viewpoint, for the CASE–4 through CASE–6 respectively. The graphs of (a-2) through (f–2) indicate the energy balance histories by each material for the CASE–1 through CASE–6 respectively. 'Body' means all the material of the Jumbo jet except for engines; 'Eng.' does all the material in the four engines; 'Con.' does all the concrete material; 'R–F' does all the reinforcement steel. On the other hand, 'Int.' stands for the internal (distortional) energy and 'Kin.' does the kinetic energy.

In every case the buckling occurs in the nose of the fuselage, and it is subjected to serious deformation. However, outstanding crashes on four engines are observed only in the CASE–1 (1 m thickness; with the reinforcement). On the contrary, every jetliner except for CASE–1 drops its main wings in the tip, like birds do when they flap. No significant deformations can be observed behind the main wings in every case.

Comparing among Fig. 16.20 (a-1) through (f-1), we can know that the concrete wall are perforated completely in the cases of CASE–1 and CASE–3 (2 m thickness; without the reinforcement). Especially, in the case of CASE–1, the both front and rear reinforcements are broken and cut in the vicinity of the impact surface. The rear reinforcements of CASE–2 seem to survive, but they are not supportable in any sense, actually some of them are known to be fractured by an additional output separately done. And outstanding spalling (scabbing) can be observed in the back side of the concrete wall of CASE–2. Slight dents or multiple shallow craters are formed around the impact area on the front side, whereas no significant deformations can be observed on the back side, for both the CASE–4 and CASE–5 that have the same thickness of 3 m.

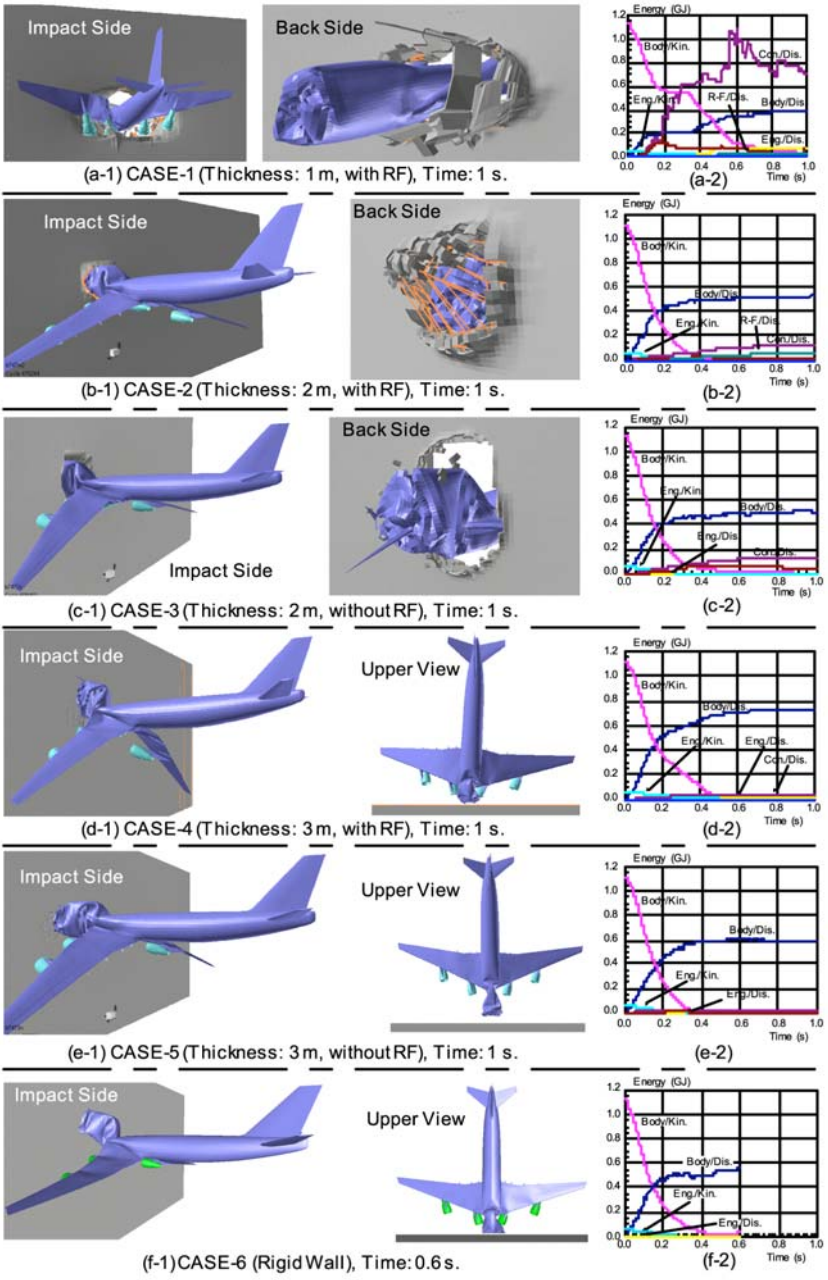

Fig. 16.20 Overview of the numerical results for five different concrete targets.